Comparing TiO_2 Nanoparticle Formulations: Stability and Photoreactivity Are Key Factors in Acute Toxicity to *Daphnia magna*

Jeffrey M. Farner, Rachel Cheong, Emeric Mahé, Hemanshu Anand, Nathalie Tufenkji*

Department of Chemical Engineering, McGill University, Montreal, Quebec, Canada
*Corresponding Author Phone: (514) 398-2999; Fax: (514) 398-6678; E-mail: nathalie.tufenkji@mcgill.ca

Environmental Significance Statement

Engineered titanium dioxide nanoparticles (TiO_2 NPs) are increasingly detected in the environment. Due to the many applications of TiO_2, formulations of different particle size, morphology, and mineral form exist that may affect the stability and toxicity of the released NPs in complex systems. Variations in behavior and impact on aquatic species amongst TiO_2 formulations remains poorly understood. This study compares two types of TiO_2 NPs in terms of photoreactivity and aggregation. The type of TiO_2, the presence of UV light, and natural organic matter are all observed to impact the toxicity to *Daphnia magna.* This work highlights the importance of considering both the aquatic chemistry and the physicochemical characteristics of the TiO_2 NPs in determining environmental risk.

TOC Art

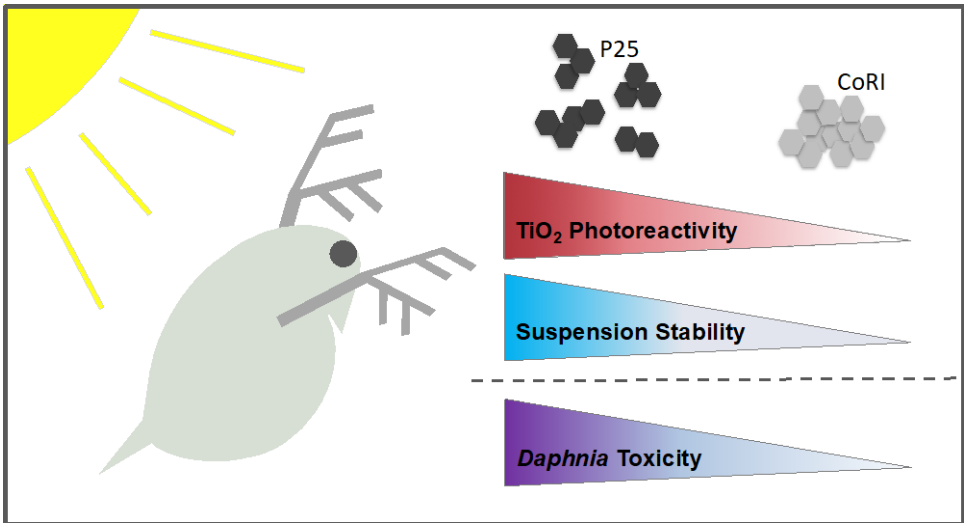

Daphnia magna toxicity is strongly influenced by the differences in photoreactivity and stability between two TiO_2 nanoparticle formulations.

Abstract

Given their widespread manufacture and use, it is anticipated that titanium dioxide nanoparticles (TiO_2 NPs) will make their way into environmental surface waters where they may adversely impact biota. Characteristics of both the NPs themselves and the aquatic environment will determine the potential risks associated with release. Here, two different commercial formulations of TiO_2 NPs are investigated in terms of aggregate stability, photoreactivity, and toxicity to the freshwater crustacean *Daphnia magna*. *D. magna* neonates were exposed to TiO_2 NPs in 48 h acute toxicity tests under either visible or UV illumination, in either the presence or absence of natural organic matter (NOM). Negligible lethal toxicity was observed by either TiO_2 formulation when illuminated by visible light, although swimming performance was significantly affected. For both NPs, the presence of UV light dramatically increased hydroxyl radical (*OH) generation and toxicity, although this was partially mitigated by the presence of NOM. Differences in toxicity between NPs are discussed in terms of stability and photoreactivity. These results show that not all TiO_2 should be treated equally, and that differences in particle stability and photoreactivity must be taken into account when predicting risk.

1. Introduction

Titanium dioxide nanoparticles (TiO_2 NPs) comprise a significant fraction of global NP production and use at the industrial scale, with estimates on the order of thousands of tons per year [1-3]. TiO_2 NPs are widely used as additives in surface coatings, paints, and cosmetic products because of their optical properties [3, 4]. Estimates suggest that 8-22 % of NPs by

mass end up in waters worldwide, during or after their use [5]. As a result, TiO_2 NP release and exposure of aquatic organisms is anticipated [6, 7]. The presence of TiO_2 NPs originating from sunscreens has been observed in waters around public beaches at tens of ppb [8], which is in keeping with estimates of expected environmental concentrations [5, 9, 10].

Given the economic interest in and widespread use of TiO_2, the ecotoxicity of TiO_2 NPs has been investigated with many animal models and algae [11-13]. *D. magna* is one common model that is particularly useful given its sensitivity and position at the base of the food web. To date, laboratory studies broadly indicate that for *D. magna*, the acute toxicity of nano-sized TiO_2 is minimal for exposures at environmentally relevant concentrations under *visible* light. Reported toxic concentrations are often on the order of hundreds of ppm and vary widely [14-18]. Moreover, TiO_2 NP stability and toxicity have been shown to depend on aquatic chemistry [19, 20].

TiO_2 is also an efficient photocatalyst, capable of producing reactive oxygen species (ROS) such as *OH when irradiated by UV light [21]. The band gap of anatase, the more photocatalytic form, is 3.2 eV, which corresponds to wavelengths less than 385 nm [22]. For *D. magna*, studies that have considered the impact of UV light observe drastic increases in toxicity [23, 24]. Mansfield et al. demonstrated that toxicity increases with the intensity of radiation using filtered natural sunlight [25]. Additionally, Wormington et al. highlighted the impact of natural organic matter (NOM) on ROS production and, thus, toxicity [26]. Understanding how commercially relevant formulations of NPs will behave following release in terms of stability in the water column, photoreactivity, and ecotoxicity will improve our understanding of risk related to TiO_2 release. While NP morphology and surface properties will impact reactivity [27], no direct comparisons between TiO_2 types have been reported. Furthermore, toxicity

studies often use different formulations of TiO_2 and different exposure media to prepare suspensions, which complicates comparison.

In this study, we compare the stability and photoreactivity of two TiO_2 NP suspensions as they impact *D. magna* toxicity. *D. magna* exposed to TiO_2 NPs were illuminated by either visible or UV-A light, both in the presence and absence of NOM. Two formulations of TiO_2 NPs were employed to assess their relative impacts on *D. magna*: the widely studied commercial P25 (80% anatase, 20% rutile) (Evonik, Germany), and a proprietary formulation composed of pure anatase and used as a paint additive, as supplied by the Coatings Research Institute (CoRI, Belgium). Photoreactivity under the different conditions was quantified through the use of a specific hydroxyl radical probe and related to observed toxicity. This work highlights the importance of TiO_2 formulation on photoreactivity, the stability of NP suspensions, and the toxicity of TiO_2 NPs.

2. Materials and Methods

TiO_2 NPs:

Experiments were performed with two formulations of TiO_2 NPs. P25 Aeroxide (Evonik, Germany) is commonly studied in the literature and is a mixture of anatase and rutile at roughly an 80:20 ratio, respectively. The second TiO_2 NP (CoRI) is a proprietary formulation composed of 95+% anatase and used as a paint additive (Coatings Research Institute, Belgium). Both formulations are comprised of uncoated TiO_2 NPs. TiO_2 NP stock suspensions were prepared at 50-200 ppm in EPA Moderately Hard Reconstituted Water (MHW) [28], which consists of 96 mg L^{-1} sodium bicarbonate (99.7+%, Sigma-Aldrich), 60 mg L^{-1} calcium sulfate dihydrate (98%, Arcos Organics), 60 mg L^{-1} magnesium sulfate (Fisher Scientific), and 4 mg L^{-1} potassium chloride (USP, Fisher Scientific). The resulting water is designed to mimic

natural, moderately hard water with a pH of 7.8. Immediately prior to use, stock suspensions were probe sonicated (Q700, QSonica, Newton, Connecticut, USA) in pulse mode (12 s on, 3 s off) for 6 min total following the NIST protocol by Taurozzi et al. [29].

Characterization:

X-ray photoelectron spectroscopy (Thermo Scientific) was used for elemental identification of TiO_2 NPs. A monochromated Al-Kα X-ray source was used with a pass energy of 200 eV and a step width of 1 eV for the survey spectra and a pass energy of 50 eV and a step width of 0.1 eV for the detailed spectra. Scans were performed with a spot size of 200 μm and the flood gun on in a 10^{-8} mbar vacuum. The aggregate size of TiO_2 suspensions was determined by Dynamic Light Scattering (DLS) with a Zetasizer Nano ZS (Malvern, Massachusetts, USA). Size measurements are reported both as intensity weighted hydrodynamic diameter and Z-average diameter (cumulants mean diameter). The heterogeneity in aggregate sizes within a suspension is indicated by the polydispersity index (PDI), which ranges from 0 to 1, with more polydisperse samples approaching unity. DLS measurements were confirmed using Transmission Electronic Microscopy (Philips CM200 TEM, Advanced Microscopy Techniques Corp.) performed on suspensions prepared on lacey carbon grids (CF400-CU, Electron Microscopy Sciences) and imaged at 200 kV. Electrophoretic mobility (EPM) measurements were collected via laser doppler velocimetry and converted to zeta potential (ZP) using the Henry equation (ZetaSizer Nano ZS, Malvern). To determine the isoelectric point (IEP), pH titrations were performed in duplicate using 100 mL suspensions of 10 ppm P25 TiO_2 in MHW. Suspensions were continually stirred while pH was monitored and adjusted with 0.1 M HCl. EPM was measured at each pH step, and the isoelectric point (IEP) was identified as the pH for which the EPM of a suspension was zero.

TiO_2 concentrations in suspension over time were measured via ICP-MS following microwave digestion (MARS 6, CEM Corp, North Carolina, USA) in sulfuric acid. 100 mL samples were prepared using the same protocol as acute toxicity tests (below) and undisturbed over the 48 h measurement period. 2 mL aliquots were taken periodically from mid height in the water column, to which 3 mL high purity sulfuric acid (96+%, Arcos Organics) was added. Samples were microwave digested at 1400 W following a 30 min ramp to 200 °C and hold time of 40 min. Following digestion, samples were diluted to a final acid concentration of 4% v/v and analyzed via ICP-MS (NexION 300X, Perkin Elmer, Massachusetts, USA). Calibrations were performed with Ti-47 isotope using the same acid matrix as the samples. Sc-45 was used as an internal standard and variation was ± 10%. Detection limits were 0.02 μg L^{-1} and background equivalent concentrations were 0.095 μg L^{-1}. Method spikes in MHW undergoing the full digestion method using a Ti-47 NIST standard provided recoveries of 76%.

TiO_2 Photoreactivity Measurements:

Photoreactivity measurements were performed under either visible (8 W fluorescent 6500K-daylight bulbs, Eiko Global, Kansas, USA) or UV light (8 W fluorescent UV lamps, peak output 365 ± 15 nm, Hikari Lamps, California, USA). The output and modeled spectra of the UV bulbs is shown in Figure S1. Samples were located under 6 bulbs placed in parallel. Because the intensity of light was greater towards the center of the bulbs, the distance from the bulbs to each beaker for UV exposure was adjusted between 15.2 and 20.3 cm to achieve the desired irradiance of 13.0 ± 0.1 W m^{-2}, as measured with a UV-radiometer (MU-200, Apogee Instruments). This UV intensity was selected as it resulted in an irradiance lower than full sun exposures, as may be encountered during cloudy days or in partially shaded waters, and it minimized the likelihood of observed *D. magna* toxicity arising solely from the

UV exposure. For comparison, a UV exposure due to sunlight of 32.4 W m^{-2} over the same wavelengths (340-390 nm) has been reported at 38 °N on a clear summer day; the total UV irradiance was 51.9 W m^{-2} (290–400 nm) [30]. Visible light exposures were performed under 4 lamps at a height of 35.6 cm and intensity of 12 μmol m^{-2} s^{-1}, measured with a MQ-200 light meter (Apogee Instruments). For visible light exposures, a small amount of UV radiation was observed (0.1-0.2 W m^{-2}, two orders of magnitude less than the irradiance used in the UV exposures).

The production of hydroxyl radicals (*OH) was monitored over 48 h using 0.5 mM terephthalic acid (TA, 99+%, Arcos Organics). Hydroxylation of the molecule produces the fluorescent 2-hydroxy terephthalic (2-HTA, 97%, Sigma-Aldrich) (ex 315 nm / em 425 nm). *OH generation under either visible or UV light was monitored for 10 ppm TiO_2 in MHW for both P25 and CoRI. For photoreactivity tests, 10 ppm sonicated TiO_2 in either the presence or absence of 10 ppm NOM was placed in MHW in 250 mL polypropylene beakers (Fisher Scientific). Suspensions were kept undisturbed in the dark at room temperature and allowed to aggregate and settle naturally. At 0, 6, 12, 24, and 48 h, suspensions were exposed to UV light in triplicate for 1 h with 1.2 mL aliquots taken every 10 min at mid height in the beaker. Suspensions were sacrificial (i.e., each beaker was only exposed to UV light once). Visible light exposures were only performed immediately after sonication (t = 0 h). Sampled aliquots were centrifuged for 5 min at 12,000 rpm (9660*g*) (MiniSpin, Eppendorf), and the supernatant was analyzed for fluorescence intensity (Fluoromax-4, Horiba Jobin Yvon). For samples containing NOM, Suwannee River NOM (Reverse Osmosis Isolate, International Humic Substances Society, USA) was added to the NP suspensions at 10 ppm. This concentration was selected as it is mid-range in concentrations common to surface waters [31]. Controls consisted of MHW and MHW with 10 ppm NOM. Fluorescence was converted to

*OH concentration using a standard curve of 2-HTA from 0.00625 – 0.125 µM, assuming a trapping efficiency of 80% [32].

The absorbance of NOM in solution at concentrations ranging from 1.25 to 100 ppm was measured via UV-Visible spectroscopy (Agilent 8453) using a 1 cm path length quartz cuvette with DI water as the blank to determine the impact of NOM on UV light penetration in the water column. The measured absorbance was then used to determine the absorption coefficient, according to the Beer-Lambert Law and the intensity of light as a function of depth was modeled.

D. magna Growth:

D. magna were obtained from Environment and Climate Change Canada and grown in MHW. 2 µg L^{-1} sodium selenate (Fisher Scientific, >99%) and 2 µg L^{-1} vitamin B12 (Fisher Scientific, 98%) were added to rear water as advised by Environment and Climate Change Canada to maintain the health of the colony[33]. These supplements were not included in test water to prevent interference with generated reactive species. *D. magna* were reared at 21 ± 1 °C and exposed to a 16 h light, 8 h dark cycle following OECD guidelines [34]. *D. magna* were fed daily with a mixture of *Chlamydomonas reinhardtii* (3.0×10^6 cells/mL) and Yeast Cerophyll^{MC} Trout (YCT) (0.8% v/v) (Aquatic Research Organisms Inc., New Hampshire, USA).

Acute Toxicity Testing:

Acute (48 h) toxicity tests were conducted according to OECD guidelines [35]. Each replicate consisted of 5 neonates (<24 h in age) placed in MHW containing various concentrations of freshly sonicated TiO_2 NPs and NOM (100 mL total volume) and exposed to either visible or UV-A light. Illumination during testing followed the same 16 h light, 8 h dark cycle used

during rearing. The concentrations tested were randomized over time, and control samples containing 5 neonates in MHW only or MHW plus 10 ppm NOM were run with each test. The addition of 10 ppm NOM was not observed to cause mortality. Temperature, pH, and dissolved oxygen content were measured in control and representative samples at the beginning and end of each test. All values conformed to OECD guidelines. Test results for a given replicate were discarded if mortality was observed in the associated control samples. At 24 and 48 h, *D. magna* were assessed and characterized as healthy, immobilized, or dead. Visual inspection of *D. magna* was performed at 10× optical microscopy (Stereomaster, Fisher Scientific). At least 4 replicates of each condition were conducted. Calculations of LC_{50} were performed on tests by fitting a sigmoidal function to the data using the Hill equation.

Swimming Performance:

Differences in *D. magna* swimming performance after exposure to visible light and TiO_2 NPs were assessed by measuring the distance traveled in one minute following the procedure outlined by Pikuda et al. [36]. 10 neonates were placed in polypropylene beakers holding 100 mL suspensions containing 1 ppm TiO_2 and exposed to the same conditions as the acute toxicity tests. After 48 h, 5 visibly healthy daphnids (i.e. freely swimming) were individually selected, placed one at a time in a small volume (1 mL) of MHW in a glass bottom culture dish containing a 1.4 cm diameter microwell (MatTek Corp), and allowed to acclimate for 2 min before being recorded for 1 min. The distance traveled by each daphnid was calculated using the Kinovea motion tracking software (www.kinovea.org). Each test was run in triplicate, resulting in 15 swimming paths collected per condition. MHW and MHW + NOM controls were run with each condition (n=30 for each). Statistical significance between treatments was determined by 1-way ANOVA followed by post-hoc Tukey's HSD ($p < 0.05$).

3. Results and Discussion

TiO_2 Characterization

K-Alpha XPS was performed on P25 and CoRI NPs deposited onto carbon tape. Figure S2 shows XPS survey scans, which did not identify the presence of any elements other than carbon (attributed to the carbon tape), oxygen and titanium for either NP, suggesting both NPs are pure TiO_2. NPs were imaged by TEM (Figure 1), and results are listed in Table 1. ImageJ analysis of TEM images indicates that the size of the primary particles differs greatly between P25 (29 ± 8 nm) and CoRI (5 ± 1 nm) (n = 100). Figures 1c and g illustrate the crystallinity of the both types of TiO2. As can be see, the lattice structure of P25 is more coherent over longer distances owing to the larger primary particle size. For P25, lattice spacings of both 0.33 nm (corresponding to the 110 Miller index of rutile) and 0.35 nm spacings (corresponding to the 101 Miller index of anatase) are observed. For CoRI, only 0.35 nm spacings (anatase) are observed.

Selected area electron diffraction (SAED) patterns for P25 and CoRI are shown in Figure 1d and h, respectively. The ring patterns are characteristic of polycrystalline samples. Analysis of the d-spacing was performed using an external calibration with aluminum diffraction standard. Identified d-spacings from diffraction rings along with their corresponding Miller indices are given in Table S3. Both TiO_2 samples exhibit diffraction patterns corresponding to anatase. The diffraction rings for CoRI are less distinct than those for P25, which could be indicative of the smaller size of CoRI NPs and electron beam passing through more areas of the NP that are amorphous (i.e. at the outer edges of the NP where lattice breaks down). That the diffraction rings of P25 also correspond to anatase is likely a function of the relative amounts of anatase (80%) and rutile (20%) in the formulation. Thus, the majority of

diffraction will be due to anatase, and diffraction corresponding to rutile may lie in the few points that can be observed between the more intense anatase rings.

DLS results shown in Table 1 highlight further differences between the suspensions. CoRI NPs form very polydisperse suspensions with a large range of sizes, as evidenced by both the high polydispersity index (> 0.80 for both CoRI and CoRI + NOM) and the difference between the Z-average diameter (order of μm) and the intensity weighted average diameter (hundreds of nm) (see Supporting Information for further discussion) [37]. While DLS is not recommended for accurate sizing of highly polydisperse suspensions [38], and results for CoRI NPs should be viewed accordingly, comparing results between the two NPs can provide insight into the differences between the two nanomaterials. The PDI of P25 and P25 + NOM is less than 0.25, suggesting these suspensions are much more monodisperse than CoRI and CoRI + NOM. Also, both the Z-average diameter and intensity weighted average diameter are between 140-240 nm, in agreement with previous observations [29, 39]. Thus, for the same aquatic chemistry and the same dispersion method, suspensions of CoRI NPs are comprised of a large range of aggregate sizes whereas aggregates of P25 NPs are generally smaller and much more monodisperse.

Table 1. TiO_2 NP characterization. All suspensions were prepared in EPA MHW and measurements performed directly after sonication (t = 0 h). Reported DLS values are averages of triplicate measurements. See Table S3 for individual results.

	[TiO_2]	**[NOM]**	**TEM**	**DLS**			**ZP**
	(mg/L)	(mg/L)	Primary particle size (d.nm)	Z-average size (d.nm)	Intensity weighted size (d.nm)	PDI	(mV)
P25	5	0	29 ± 8	167	188	0.21	-16.4 ± 0.7
P25 + NOM	5	10		142	233	0.22	-18.8 ± 0.8
CoRI	5	0	5 ± 1	2598	354	0.86	-20.1 ± 0.7
CoRI + NOM	5	10		2467	379	0.82	-22.0 ± 1.4

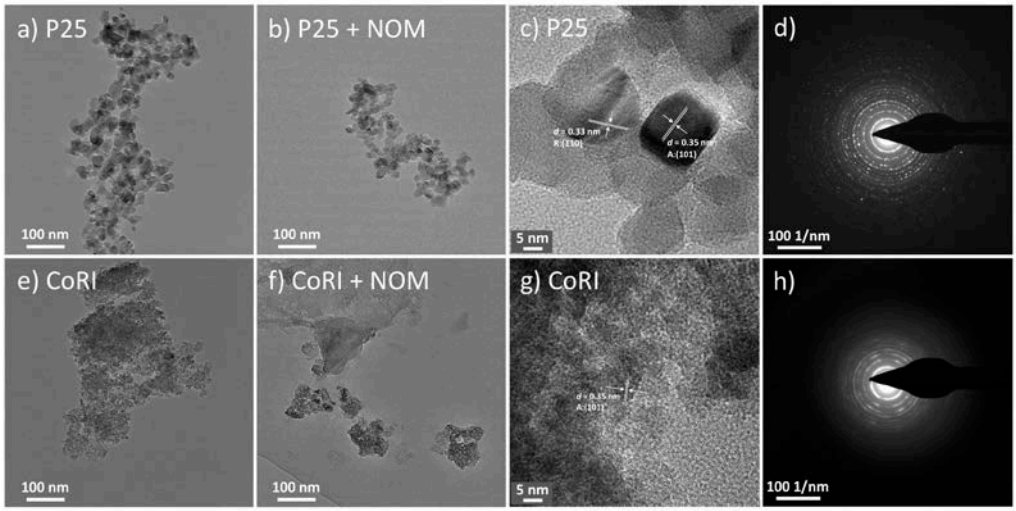

Figure 1. TEM images of TiO_2 NPs suspended at 5 ppm in MHW: a) bare P25, b) P25 in 10 ppm NOM, c) high resolution of P25, d) ring diffraction from P25 e) bare CoRI, f) CoRI in 10 ppm NOM, g) high resolution of CoRI, h) ring diffraction of CoRI.

In all test conditions, measurements of EPM indicated negatively charged particles, which was expected given the pH of MHW at 7.8 is above the point of zero charge (pzc) of TiO_2 (approx. 6 for bare anatase) [40]. Considerable differences were observed in the isoelectric points (IEPs) of P25 and CoRI in MHW in this study. ZP vs pH titrations are shown in Figure S5. The IEP of P25 was observed to be approximately 5.8, which agrees well with previous results for P25 in the presence of sulfate (where the IEP of P25 in nitrate or chloride was 6.6) [39]. In contrast, the IEP of CoRI was not observed, occurring at a pH < 3. While the difference in the ZP vs pH titrations could be indicative of differences in surface coatings or surface passivation, XPS results do not show the presence of any other elements beyond titanium and oxygen. These deviations may be due to the anionic species present in MHW, namely carbonate and sulfate. Previously, both anions were observed to undergo inner sphere ligand exchange and alter the IEP of P25, with carbonate having a particularly strong impact [39]. The shift in IEP suggests that CoRI NPs may more readily interact with carbonate than P25. The presence of NOM had a negligible impact on surface charge (Table 1).

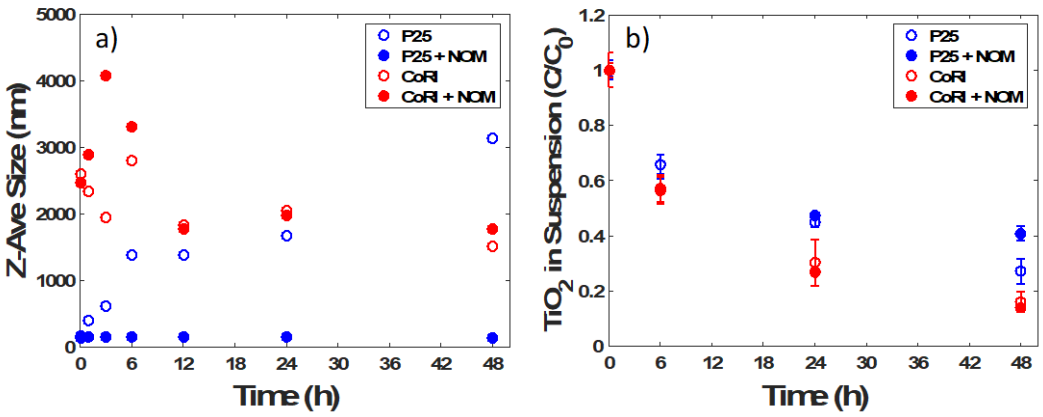

Figure 2. a) Time-resolved DLS data of TiO_2 suspensions. Aggregate size versus time for P25 or CoRI NPs suspended in MHW or MHW supplemented with 10 ppm NOM. b) Normalized ICP-MS measurements of TiO_2 concentration remaining in suspension (measured as Ti) versus time.

Time resolved DLS (TRDLS) data, plotted as Z-average size (Figure 2a), indicate that the TiO_2 suspensions exhibit a range of stabilities. P25 NPs, though initially forming small aggregates, are largely unstable in MHW and undergo significant aggregation over the first 6 h. The z-average size increases from approximately 160 nm initially to the micron range after 48 h. However, in the presence of 10 ppm NOM (P25 + NOM), the P25 NPs are quite stable, with no change in DLS size over the 48 h period. Despite this, a decrease in count rate (Figure S6) suggests that some deposition occurs as aggregates begin to settle outside the path of the laser, resulting in the decreased scattering of incident photons. Z-average values for CoRI NP aggregates are initially much larger, on the order of microns, but decrease over time. Given that samples are not stirred, and thus breakup of aggregates is not expected, these results suggest significant settling of the largest fraction over time (Figure 2a). In contrast to P25, the presence of NOM had no discernable impact on CoRI stability.

To further determine the stability of the TiO_2 NPs in MHW, ICP-MS was performed on aliquots sampled at 0, 6, 24, and 48 h from mid height in a 250 mL polypropylene beaker (Figure 2b). The concentration of all NPs, nominally 1 ppm at t = 0 h, drastically decreased

over time. In agreement with TRDLS results, P25 + NOM exhibited the least amount of loss, with 41 ± 3% remaining in the water column, compared to P25 by itself (27 ± 5%). CoRI NPs were less stable than P25 NPs. After 48 h, 16 ± 4% and 14 ± 2% of CoRI and CoRI + NOM remained in the water column, respectively. These results agree with observations by Ma et al. who report up to 67 % loss over 24 h with P25 in MHW at a starting concentration of 7 ppm [24].

Thus, for all conditions, the concentration of TiO_2 NPs is expected to decrease over time during 48 h *D. magna* exposures. The influence of NOM may be to stabilize the smallest fraction, limiting aggregation, though particles will still be subject to settling. For P25, where the initial suspension is made of smaller, more homogeneous aggregates, this influence is more pronounced. Calculations of Stokes' settling velocities (Figure S7) suggest that aggregates larger than 950 nm (diameter) will settle the full distance of the water column (13.8 cm) over 48 h. Aggregates larger than 675 nm will settle half the height of the water column in 48 h. While some resuspension and bioturbation would be expected due to the swimming action of *D. magna* in the beaker, the 48 h duration of the test suggests that most particles will be susceptible to settling. At the highest TiO_2 NP concentrations, settling of TiO_2 was visually observed as a white deposit on the bottom of beakers.

TiO_2 Photoreactivity

NP photoreactivity tests were performed using the same lighting conditions employed during toxicity testing. *OH were detected by measuring the increase in fluorescence resulting from the hydroxylation of TA to 2-HTA. These fluorescence measurements were then converted to *OH generation rates through the use of a 2-HTA standard curve (Figure S8). P25, which is known for its photocatalytic ability, was observed to be much more

photoactive than CoRI when exposed to UV light (Figure 3a). P25 produced *OH in the bulk suspension at an initial rate of 45.7 ± 3.9 nM min^{-1}. In contrast, the initial rate of *OH generation for CoRI was 1.9 ± 0.1 nM min^{-1}.

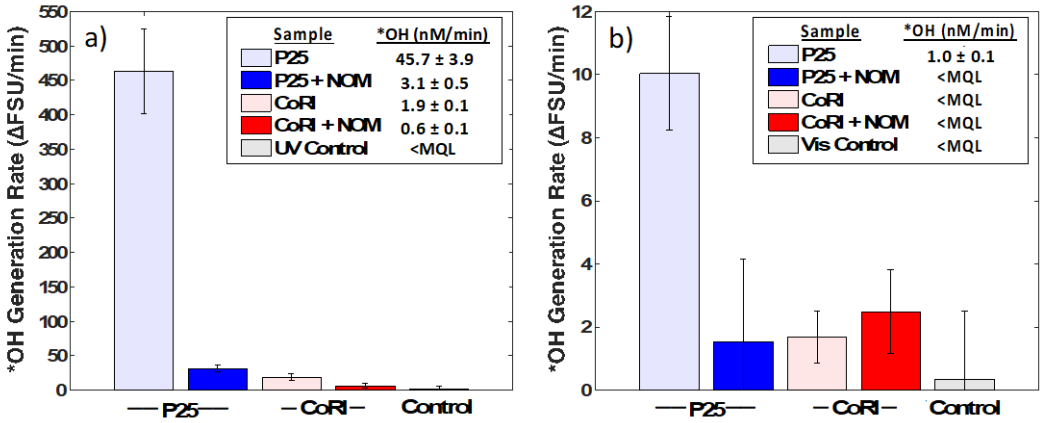

Figure 3. *OH generation rates plotted as change in fluorescence over time for 10 ppm TiO_2 as a function of NP type and presence/absence of NOM under a) UV light and b) visible light conditions used in *D. magna* toxicity tests. *OH generation rates (nM/min) calculated from 2-HTA standard curves are listed in the legends. Samples for which fluorescence values were below the minimum quantification limit are listed as <MQL. Note, y-axis scales are different, with P25 generating greater *OH than CORI.

The presence of NOM reduced initial *OH production by nearly an order of magnitude for both types of NPs to 3.1 ± 0.5 and 0.6 ± 0.1 nM min^{-1} for P25 + NOM and CoRI + NOM, respectively. As TA provides a measure of *OH in the bulk solution [41], a reduction in fluorescence may arise from the chromaphoric NOM either absorbing incident UV light prior to TiO_2 photocatalysis or quenching the radical after photocatalytic generation. Wormington et al. showed that, in a 250 mL crystallizing dish, 10 ppm NOM was observed to reduce UV intensity by 17%, providing evidence that the primary impact of NOM is due to ROS quenching [26].

By measuring the absorbance of NOM at multiple concentrations in solution, we calculated the absorption coefficient of NOM ($\alpha_{NOM,\lambda}$) for the UV bulb output and modeled the UV

intensity as a function of depth in the beaker (see Supporting Information, Figure S10). In the presence of NOM, the total intensity of UV light at the bottom of the beaker (3.71 W m^{-2}) is only 28.5 % that of the upper surface. The spatial average of UV light intensity in the water column was calculated to be 7.58 W m^{-2}, or 57.9% the intensity at the surface. The contribution to light attenuation from MHW itself was negligible. Using these calculations and the observed *OH generation rate of 45.7 nM min^{-1} for P25, some insight into the relative impact of light attenuation and *OH quenching can be obtained. If a decrease in *OH production was due solely to light attenuation, the generation rate of P25 + NOM would be anticipated to be 26.5 nM min^{-1}. The measured rate of 3.1 ± 0.5 nM min^{-1} is substantially less than what the decrease in UV intensity would merit, suggesting a significant contribution due to radical quenching. Both light attenuation and quenching will produce the same effect: a decreased delivery of the radical to a given target (e.g., *D. magna*). While NOM is itself a known photocatalyst, capable of producing ROS (e.g., singlet oxygen [42]), no *OH production was detected in controls containing only 10 ppm NOM. Overall, *OH generation under UV light followed the trend of P25 > P25 + NOM > CORI > CoRI + NOM.

*OH production was measured over 48 h in beakers that were otherwise undisturbed, allowing TiO_2 NPs to aggregate and settle naturally (Figure 4). The results show the anticipated evolution in *OH exposure for *D. magna* over time. For CoRI and P25 NPs in the absence of NOM, a strong decrease in *OH generation over time is observed that agrees with measured concentration and aggregation data. While the generation rate is less for NPs + NOM, the decrease over time is not as pronounced. In particular, P25 + NOM, which after 48 h had the largest remaining concentration in suspension (41 ± 3%) showed no change in *OH production over time. Because ROS production is inversely correlated to the size of aggregate, the smallest aggregates will be responsible for the majority of ROS production, and the net

ROS production of a suspension will decrease as NPs aggregate [43, 44]. Thus, the average concentration of *OH in suspension will decrease over time due to both the aggregation and settling of NPs. It's likely that NOM is stabilizing the smallest fraction of aggregates which then continue to produce *OH at roughly the same rate over 48 h. Despite this stabilization, even at 48 h, *OH production for both P25 and CoRI in the absence of NOM remains greater than in the presence of NOM.

*OH production was also monitored under visible light exposure, with only P25 resulting in a *OH generation rate (1.0 ± 0.1 nM min^{-1}) that was statistically different from the control ($p < 0.05$). All other conditions were below the minimum quantification limit (< MQL) of the standard curve (Figure 3b). This small amount of radical generation in P25 likely arises due to the slight emission of the fluorescent bulbs that exists at energies above the band gap of TiO_2 (3.2 eV for anatase, 3.1-3.3 eV for P25) [39].

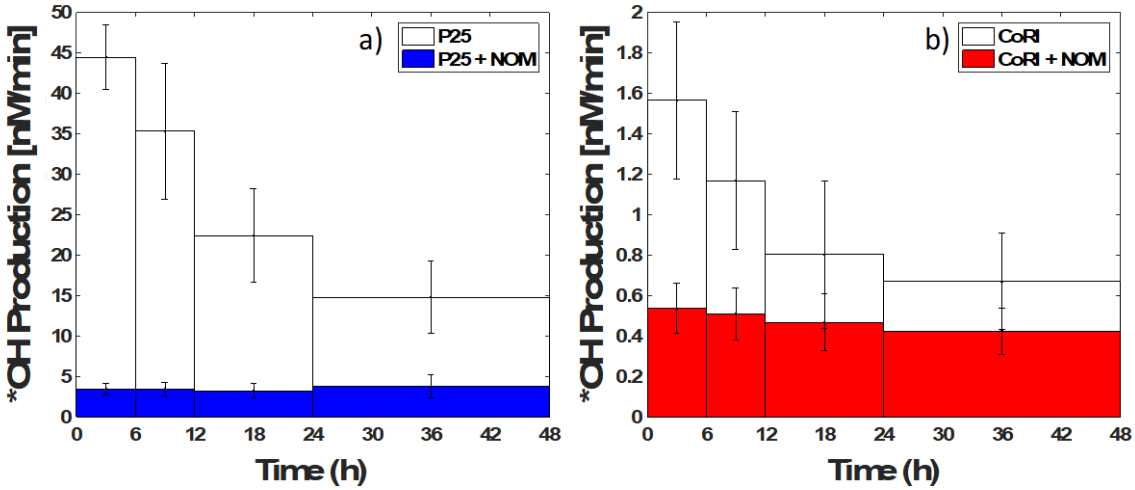

Figure 4. *OH generation rates (μM/min) for a) 10 ppm P25 and b) CoRI over 48 h as a function of NP type and presence/absence of NOM under UV light (13.1 W/m^2). Values shown are averages of the measured generation rates ± std. Note, y-axis scales are different, with P25 generating greater *OH than CORI.

D. magna Toxicity Under Visible Light

D. magna exposed to TiO_2 NPs under visible light displayed little toxicity (Figure 5a). Rapid aggregation and sedimentation were observed for bare TiO_2 suspensions, with visible deposits forming at the bottom of the beakers after a few hours for concentrations of 50 ppm and higher. When observing *D. magna*, care was taken not to disturb or mix the beakers so as to limit resuspension of aggregated and settled NPs. For P25, a low level of toxicity was observed at concentrations as low as 1 ppm, though this did not greatly increase even at 100 ppm. The maximum mortality was observed to be roughly 50 % after 48 h in 100 ppm P25. The addition of NOM to suspensions reduced the observed mortality, with only minimal (< 10%) effects observed for P25 + NOM at 10 and 25 ppm TiO_2. For CoRI NPs, slight toxicity (up to 20%) was observed at concentrations above 10 ppm; however, again this effect was mitigated by the presence of NOM. No toxicity was observed at any concentration for CoRI + NOM.

In the absence of UV light, any observed toxicity should be due to the particles themselves rather than their photocatalytic ability. Although these results would appear to suggest that P25 may be slightly more toxic than CoRI, the impact of P25 may be due to the observed low levels of *OH generated under visible light. The fact that toxicity was observed for CoRI NPs only above 10 ppm supports that there is little inherent acute toxicity due to the TiO_2 NPs themselves and agrees with previous reports where acute toxicity is only observed at unrealistically elevated concentrations [14, 16, 18].

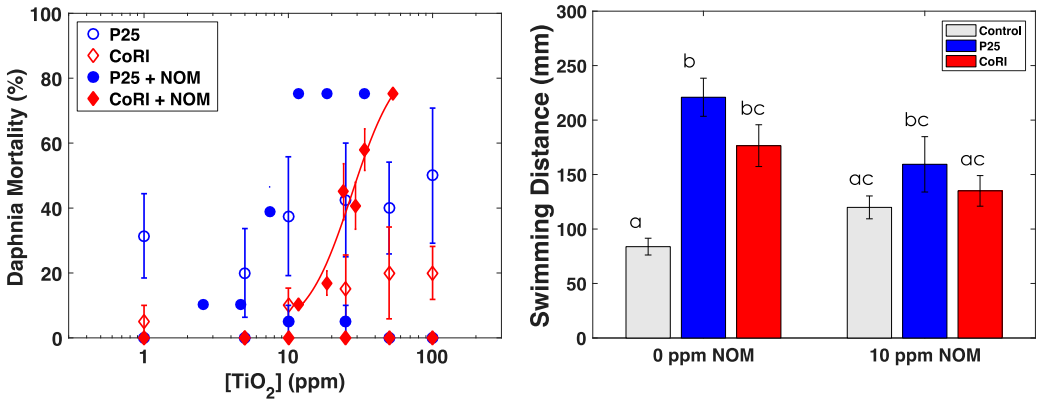

Figure 5. a) *D. magna* mortality after 48 h exposure to NPs under visible light. Error bars represent standard error (n≥4), b) Distance covered by *D. magna* in 1 min following 48 h exposure to 1 ppm TiO_2 and visible light. Error bars are standard error (n=15 for P25 and CoRI, n=30 for controls). Letters denote statistical differences ($p < 0.05$) determined by 1-way ANOVA followed by post-hoc Tukey's HSD.

Swimming Performance

While 100 % mortality was not observed for TiO_2 under visible light at any of the concentrations studied, other sublethal toxicity metrics such as swimming performance provide more sensitive endpoints for analyzing impact [45]. Figure 5b presents the average distance covered in 1 min by *D. magna* following 48 h exposure to 1 ppm TiO_2 NPs under visible light, and example swimming traces are shown in Figure S12. *D. magna* exposed to only TiO_2 NPs exhibited statistically greater swimming activity (221.0 ± 17.5 mm and 176.5 ± 19.2 for P25 and CoRI, respectively) than *D. magna* in only MHW (83.8 ± 7.7 mm) (values reported as average ± standard error). The difference was not significant, however, between TiO_2 NPs + NOM (159.4 ± 25.4 mm and 135.0 ± 14.0 for P25 and CoRI, respectively) and the MHW + NOM control (127.6 ± 16.1 mm). Thus, the presence of TiO_2 alone causes an increase in swimming activity, which may be a result of the *D. magna* attempting to escape a low level stressor, resulting in an increased depletion of energy reserves and making predation more likely [45]. These results suggest that, while acute toxicity is not observed even at unrealistically high concentrations, further study into how TiO_2 may alter *D. magna* behavior is warranted.

D. magna Toxicity Under UV light

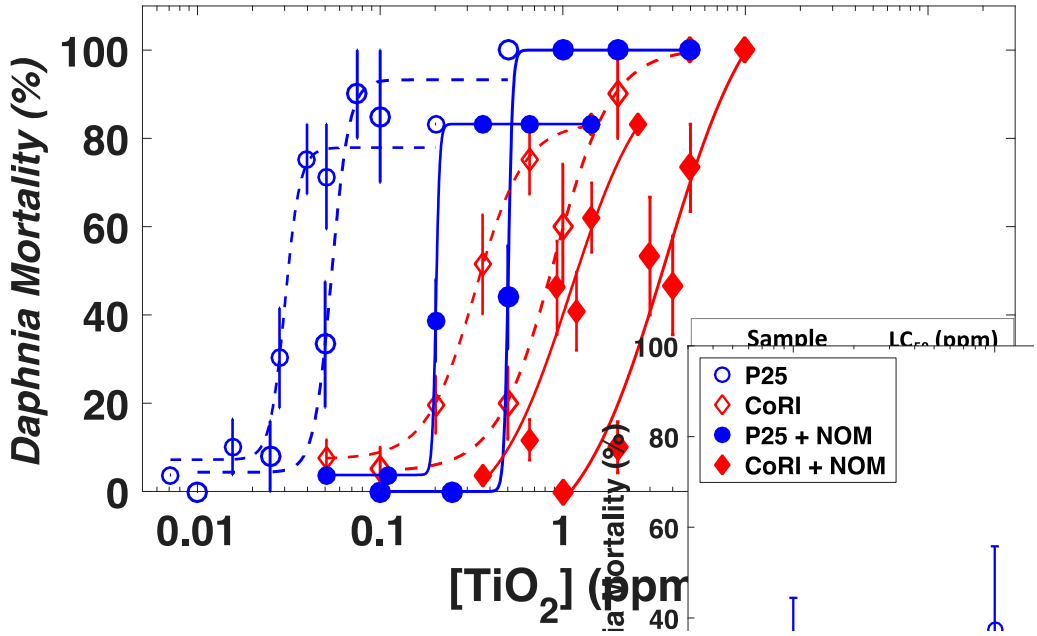

Figure 6. *D. magna* mortality versus TiO_2 NP concentration under UV light. Error bars indicate standard error. (n = at least 4 runs as per OECD test protocol).

Figure 6 shows *D. magna* mortality versus TiO_2 concentration for organisms exposed to NPs while illuminated by UV light. In comparison to visible light results, very clear dose-response curves are observed for UV exposed TiO_2. Overall, *D. magna* toxicity under UV light followed the trend of P25 > P25 + NOM > CoRI > CoRI + NOM. These results mirror trends observed for *OH generation. The LC_{50} for P25 (0.05 ppm) is an order of magnitude lower than that of CoRI (0.90 ppm) or P25 + NOM (0.50 ppm). For CoRI + NOM, the LC_{50} is on the order of ppm (3.67 ppm). As can be observed in all cases, P25 is more toxic than CoRI NPs. Additionally, the presence of NOM drastically reduces toxicity for a given NP type. This agrees well with the decrease in *OH observed in the presence of NOM, both here and in previous reports where the presence of NOM has generally been shown to have a protective effect for

organisms exposed to TiO_2 [26, 46-48]. The LC_{50} for CoRI (0.90 ppm) is comparable to that reported by Wormington et al. for pure anatase in the absence of NOM (0.84 ppm) [26].

The steepness of the dose-response curve generally indicates the potency of the toxicant, suggesting that P25, even in the presence of NOM, is more "potent" than CoRI when exposed to UV light. This is especially apparent when comparing P25 + NOM and CoRI, where the range of TiO_2 concentrations in which P25 + NOM exhibits a response but not 100% mortality is much narrower than for CoRI. This may be related to the stability of P25 + NOM in suspension, as mortality is observed at the end of 48 h. Thus, despite the similar initial *OH generation rates (3.1 ± 0.5 nM min^{-1} for P25 + NOM, 1.9 ± 0.1 nM min^{-1} for CoRI), the loss of CoRI NPs from suspension over time results in a significant decrease in the cumulative *OH dose the *D. magna* are exposed to, reducing the observed mortality. In contrast, *OH generation for P25 + NOM is observed to be fairly constant over the 48 h.

It should be noted that differences in bioaccumulation and depuration between P25 and CoRI NPs (e.g. NP shape, aggregate size) may impact the observed toxicity. While bioaccumulation was not measured in this work, no trend in mortality was observed for NPs in visible light which suggests that *OH production is the critical component in acute toxicity. However, a greater NP body burden could add an additional stress to the organism, increasing its susceptibility. Additionally, the presence of NOM, which here is linked to *OH quenching and changes in the stability of P25 aggregates, may influence the *D. magna* body burden compared to the same NP in the absence of NOM.

4. Conclusions

Concentrations of bare TiO_2 NPs that are acutely toxic to *D. magna* under visible light conditions are found to be higher than what is realistically expected in environmental waters. However, at NP concentrations in which 100% mortality is not observed, *D. magna* exhibit behavioral changes that suggest the potential for ecosystem impacts. UV light exposure drastically increases toxicity, reducing the calculated LC_{50}. For P25, this value (50 ppb) is on the same order of magnitude as upper limit aquatic measurements and falls within environmental relevance (tens of ppb) [5, 8-10]. The presence of 10 ppm NOM is observed to reduce toxicity. In natural environments, both organic matter and sunlight are likely to be present. The mitigating impact of NOM, however, is not sufficient to fully counterbalance the enhanced toxicity associated with photoexcitation. Furthermore, these results also underscore that not all TiO_2 should be considered the same. Differences in NP stability and photoreactivity are observed between the two formulations, and these factors should be taken into account when assessing risk. While toxicity related solely to the particles themselves are roughly the same for P25 and CoRI, P25 is shown to be more toxic under UV irradiation than CoRI.

5. Acknowledgements

The authors acknowledge the financial support of the Canada Research Chairs program, the Natural Sciences and Engineering Research Council of Canada, Environment and Climate Change Canada, and the Coatings Research Institute. The authors thank G. Farley, M. Houde, and M. Giraudo at Environment and Climate Change Canada for providing the source *D. magna* and consultation in rearing, A. Azimzada for performing ICP-MS measurements, K. J. Wilkinson for providing access to the ICP-MS, and L. M. Hernandez for performing TEM imaging and XPS, and D. Liu at the Facility for Electron Microscopy Research of McGill University for help in microscope operation and data collection.

6. References

1. Robichaud, C. O.; Uyar, A. E.; Darby, M. R.; Zucker, L. G.; Wiesner, M. R., Estimates of upper bounds and trends in nano-TiO2 production as a basis for exposure assessment. *Environ Sci Technol* **2009,** *43*, (12), 4227-4233.
2. Hendren, C. O.; Mesnard, X.; Droge, J.; Wiesner, M. R., Estimating production data for five engineered nanomaterials as a basis for exposure assessment. *Environ Sci Technol* **2011,** *45*, (7), 2562-9.
3. Piccinno, F.; Gottschalk, F.; Seeger, S.; Nowack, B., Industrial production quantities and uses of ten engineered nanomaterials in Europe and the world. *J Nanopart Res* **2012,** *14*, (9).
4. Al-Kattan, A.; Wichser, A.; Zuin, S.; Arroyo, Y.; Golanski, L.; Ulrich, A.; Nowack, B., Behavior of TiO2 released from nano-TiO2-containing paint and comparison to pristine nano-TiO2. *Environ Sci Technol* **2014,** *48*, (12), 6710-6718.
5. Keller, A. A.; Lazareva, A., Predicted Releases of Engineered Nanomaterials: From Global to Regional to Local. *Environmental Science & Technology Letters* **2014,** *1*, (1), 65-70.
6. Bottero, J.-Y.; Auffan, M.; Borschnek, D.; Chaurand, P.; Labille, J.; Levard, C.; Masion, A.; Tella, M.; Rose, J.; Wiesner, M. R., Nanotechnology, global development in the frame of environmental risk forecasting. A necessity of interdisciplinary researches. *Comptes Rendus Geoscience* **2015,** *347*, (1), 35-42.
7. Sun, T. Y.; Mitrano, D. M.; Bornhöft, N. A.; Scheringer, M.; Hungerbühler, K.; Nowack, B., Envisioning Nano release dynamics in a changing world: using dynamic probabilistic modeling to assess future environmental emissions of engineered nanomaterials. *Environ Sci Technol* **2017,** *51*, (5), 2854-2863.
8. Gondikas, A. P.; Kammer, F. v. d.; Reed, R. B.; Wagner, S.; Ranville, J. F.; Hofmann, T., Release of TiO2 nanoparticles from sunscreens into surface waters: a one-year survey at the old Danube recreational Lake. *Environ Sci Technol* **2014,** *48*, (10), 5415-5422.
9. Gottschalk, F.; Sonderer, T.; Scholz, R. W.; Nowack, B., Modeled environmental concentrations of engineered nanomaterials (TiO2, ZnO, Ag, CNT, fullerenes) for different regions. *Environ Sci Technol* **2009,** *43*, (24), 9216-9222.
10. Kiser, M.; Westerhoff, P.; Benn, T.; Wang, Y.; Perez-Rivera, J.; Hristovski, K., Titanium nanomaterial removal and release from wastewater treatment plants. *Environ Sci Technol* **2009,** *43*, (17), 6757-6763.
11. Sharma, V. K., Aggregation and toxicity of titanium dioxide nanoparticles in aquatic environment—a review. *Journal of Environmental Science and Health Part A* **2009,** *44*, (14), 1485-1495.
12. Schultz, A. G.; Boyle, D.; Chamot, D.; Ong, K. J.; Wilkinson, K. J.; McGeer, J. C.; Sunahara, G.; Goss, G. G., Aquatic toxicity of manufactured nanomaterials: challenges and recommendations for future toxicity testing. *Environmental Chemistry* **2014,** *11*, (3), 207-226.
13. Menard, A.; Drobne, D.; Jemec, A., Ecotoxicity of nanosized TiO2. Review of in vivo data. *Environmental pollution* **2011,** *159*, (3), 677-684.
14. Heinlaan, M.; Ivask, A.; Blinova, I.; Dubourguier, H.-C.; Kahru, A., Toxicity of nanosized and bulk ZnO, CuO and TiO 2 to bacteria Vibrio fischeri and crustaceans Daphnia magna and Thamnocephalus platyurus. *Chemosphere* **2008,** *71*, (7), 1308-1316.
15. Wiench, K.; Wohlleben, W.; Hisgen, V.; Radke, K.; Salinas, E.; Zok, S.; Landsiedel, R., Acute and chronic effects of nano-and non-nano-scale TiO2 and ZnO particles on mobility

565 and reproduction of the freshwater invertebrate Daphnia magna. *Chemosphere* **2009,** *76*,
566 (10), 1356-1365.
567 16. Zhu, X.; Chang, Y.; Chen, Y., Toxicity and bioaccumulation of TiO2 nanoparticle
568 aggregates in Daphnia magna. *Chemosphere* **2010,** *78*, (3), 209-215.
569 17. Jacobasch, C.; Völker, C.; Giebner, S.; Völker, J.; Alsenz, H.; Potouridis, T.; Heidenreich,
570 H.; Kayser, G.; Oehlmann, J.; Oetken, M., Long-term effects of nanoscaled titanium dioxide on
571 the cladoceran Daphnia magna over six generations. *Environmental pollution* **2014,** *186*,
572 180-186.
573 18. Salieri, B.; Pasteris, A.; Baumann, J.; Righi, S.; Köser, J.; D'Amato, R.; Mazzesi, B.; Filser,
574 J., Does the exposure mode to ENPs influence their toxicity to aquatic species? A case study
575 with TiO 2 nanoparticles and Daphnia magna. *Environmental Science and Pollution Research*
576 **2015,** *22*, (7), 5050-5058.
577 19. Hsiung, C.-E.; Lien, H.-L.; Galliano, A. E.; Yeh, C.-S.; Shih, Y.-h., Effects of water chemistry
578 on the destabilization and sedimentation of commercial TiO2 nanoparticles: Role of double-
579 layer compression and charge neutralization. *Chemosphere* **2016,** *151*, 145-151.
580 20. Cupi, D.; Hartmann, N. B.; Baun, A., Influence of pH and media composition on
581 suspension stability of silver, zinc oxide, and titanium dioxide nanoparticles and
582 immobilization of Daphnia magna under guideline testing conditions. *Ecotoxicology and*
583 *environmental safety* **2016,** *127*, 144-152.
584 21. Hoffmann, M. R.; Martin, S. T.; Choi, W. Y.; Bahnemann, D. W., Environmental
585 Applications of Semiconductor Photocatalysis. *Chem Rev* **1995,** *95*, (1), 69-96.
586 22. Hoffmann, M.; Hotze, E. M.; Wiesner, M. R., Reactive oxygen species generation on
587 nanoparticulate material. *Environmental Nanotechnology. Applications and Impacts of*
588 *Nanomaterials* **2007**, 155-203.
589 23. Clemente, Z.; Castro, V.; Jonsson, C.; Fraceto, L., Minimal levels of ultraviolet light
590 enhance the toxicity of TiO 2 nanoparticles to two representative organisms of aquatic
591 systems. *J Nanopart Res* **2014,** *16*, (8), 2559.
592 24. Ma, H.; Brennan, A.; Diamond, S. A., Phototoxicity of TiO2 nanoparticles under solar
593 radiation to two aquatic species: Daphnia magna and Japanese medaka. *Environ Toxicol Chem*
594 **2012,** *31*, (7), 1621-1629.
595 25. Mansfield, C.; Alloy, M.; Hamilton, J.; Verbeck, G.; Newton, K.; Klaine, S.; Roberts, A.,
596 Photo-induced toxicity of titanium dioxide nanoparticles to Daphnia magna under natural
597 sunlight. *Chemosphere* **2015,** *120*, 206-210.
598 26. Wormington, A. M.; Coral, J.; Alloy, M. M.; Delmarè, C. L.; Mansfield, C. M.; Klaine, S. J.;
599 Bisesi, J. H.; Roberts, A. P., Effect of natural organic matter on the photo‐induced toxicity of
600 titanium dioxide nanoparticles. *Environ Toxicol Chem* **2017,** *36*, (6), 1661-1666.
601 27. Dufour, F.; Pigeot-Remy, S.; Durupthy, O.; Cassaignon, S.; Ruaux, V.; Torelli, S.; Mariey,
602 L.; Maugé, F.; Chanéac, C., Morphological control of TiO 2 anatase nanoparticles: What is the
603 good surface property to obtain efficient photocatalysts? *Applied Catalysis B: Environmental*
604 **2015,** *174*, 350-360.
605 28. EPA, U. *Methods for measuring the acute toxicity of effluents and receiving waters to*
606 *freshwater and marine organisms*; EPA/600/4-90: 1993.
607 29. Taurozzi, J.; Hackley, V.; Wiesner, M., Preparation of a nanoscale TiO2 aqueous
608 dispersion for toxicological or environmental testing. *NIST Special Publication* **2012,** *1200*, 3.
609 30. Diffey, B. L., Sources and measurement of ultraviolet radiation. *Methods* **2002,** *28*, (1),
610 4-13.
611 31. Crittenden, J. C.; Trussell, R. R.; Hand, D. W.; Howe, K. J.; Tchobanoglous, G., *MWH's*
612 *Water Treatment: Principles and Design: Principles and Design*. John Wiley & Sons: 2012.

32. Ishibashi, K.-i.; Fujishima, A.; Watanabe, T.; Hashimoto, K., Quantum yields of active oxidative species formed on TiO2 photocatalyst. *Journal of Photochemistry and Photobiology A: Chemistry* **2000,** *134*, (1), 139-142.
33. Canada, E., Biological test method: Reference method for determining acute lethality of effluents to Daphnia magna. **1990**.
34. Co-operation, O. f. E.; Development, *Test No. 202: Daphnia sp. Acute Immobilisation Test*. OECD Publishing: 2004.
35. No, O. T., 202: Daphnia sp. acute immobilisation test. *OECD guidelines for the testing of chemicals, section* **2004,** *2*.
36. Pikuda, O.; Xu, E. G.; Berk, D.; Tufenkji, N., Toxicity Assessments of Micro- and Nanoplastics Can Be Confounded by Preservatives in Commercial Formulations. *Environmental Science & Technology Letters* **2018,** *6*, (1), 21-25.
37. Bhattacharjee, S., DLS and zeta potential–What they are and what they are not? *Journal of Controlled Release* **2016,** *235*, 337-351.
38. Domingos, R. F.; Baalousha, M. A.; Ju-Nam, Y.; Reid, M. M.; Tufenkji, N.; Lead, J. R.; Leppard, G. G.; Wilkinson, K. J., Characterizing manufactured nanoparticles in the environment: multimethod determination of particle sizes. *Environ Sci Technol* **2009,** *43*, (19), 7277-7284.
39. Farner Budarz, J.; Turolla, A.; Piasecki, A. F.; Bottero, J.-Y.; Antonelli, M.; Wiesner, M. R., Influence of aqueous inorganic anions on the reactivity of nanoparticles in TiO2 photocatalysis. *Langmuir* **2017,** *33*, (11), 2770-2779.
40. Kosmulski, M., The significance of the difference in the point of zero charge between rutile and anatase. *Adv Colloid Interfac* **2002,** *99*, (3), 255-264.
41. Turolla, A.; Piazzoli, A.; Farner Budarz, J.; Wiesner, M. R.; Antonelli, M., Experimental measurement and modelling of reactive species generation in TiO2 nanoparticle photocatalysis. *Chemical Engineering Journal* **2015,** *271*, 260-268.
42. Latch, D. E.; McNeill, K., Microheterogeneity of singlet oxygen distributions in irradiated humic acid solutions. *Science* **2006,** *311*, (5768), 1743-1747.
43. Jassby, D.; Budarz, J. F.; Wiesner, M., Impact of Aggregate Size and Structure on the Photocatalytic Properties of TiO2 and ZnO Nanoparticles. *Environ Sci Technol* **2012,** *46*, (13), 6934-6941.
44. Hotze, E. M.; Bottero, J. Y.; Wiesner, M. R., Theoretical Framework for Nanoparticle Reactivity as a Function of Aggregation State. *Langmuir* **2010,** *26*, (13), 11170-11175.
45. Lovern, S. B.; Strickler, J. R.; Klaper, R., Behavioral and physiological changes in Daphnia magna when exposed to nanoparticle suspensions (titanium dioxide, nano-C60, and C60HxC70Hx). *Environ Sci Technol* **2007,** *41*, (12), 4465-4470.
46. Seitz, F.; Rosenfeldt, R. R.; Müller, M.; Lüderwald, S.; Schulz, R.; Bundschuh, M., Quantity and quality of natural organic matter influence the ecotoxicity of titanium dioxide nanoparticles. *Nanotoxicology* **2016,** *10*, (10), 1415-1421.
47. Yang, S. P.; Bar-Ilan, O.; Peterson, R. E.; Heideman, W.; Hamers, R. J.; Pedersen, J. A., Influence of humic acid on titanium dioxide nanoparticle toxicity to developing zebrafish. *Environ Sci Technol* **2013,** *47*, (9), 4718-4725.
48. Li, S.; Ma, H.; Wallis, L. K.; Etterson, M. A.; Riley, B.; Hoff, D. J.; Diamond, S. A., Impact of natural organic matter on particle behavior and phototoxicity of titanium dioxide nanoparticles. *Sci Total Environ* **2016,** *542*, 324-333.